Eur. Phys. J. Special Topics **222**, 2571–2582 (2013)

DOI: 10.1140/epjst/e2013-02038-3

THE EUROPEAN PHYSICAL JOURNAL SPECIAL TOPICS

Regular Article

Synchronization in the network of chaotic microwave oscillators

O. Moskalenko[1,2], N. Phrolov[1], A. Koronovskii[1,2], and A. Hramov[1,2,a]

[1] Saratov State University, Saratov, Russia
[2] Saratov State Technical University, Saratov, Russia

Received 16 July 2013 / Received in final form 13 August 2013
Published online 28 October 2013

Abstract. Time scale synchronization in networks of chaotic microwave oscillators with the different topologies of the links between nodes has been studied. As a node element of the network the one-dimensional distributed model of the low-voltage vircator has been used. To characterize the degree of synchronization in the whole network the synchronization index has been introduced. The transition to the synchronous regime is shown to take place via cluster time scale synchronization. Meanwhile, the spectral structure of the output signals is complicated sufficiently which allows using such devices in a number of practical applications.

1 Introduction

Chaotic synchronization is one of the fundamental phenomena, widely studied recently, having both the theoretical and applied significance [1–3]. For example, chaotic synchronization can be used for the secure information transmission [4–6] and control of chaotic systems [7–9]. One of the promising fields of the use of synchronization phenomena is generation, receiving and processing of GHz–THz complex signals by means of the nonlinear antenna technology [10]. Nonlinear antennas are inherently nonlinear dynamic systems consisting of the set of coupled microwave generators with complex dynamics, for example, solid state devices or beam-plasma systems [11–15]. It is well-known that such coupled systems can demonstrate a number of unusual nonlinear phenomena [16–20], therefore there is a need of developing novel approaches and techniques for the analysis and control of cooperative dynamics (including chaotic synchronization) of coupled microwave oscillators for the active antenna design [8,21–23].

At present, several different types of chaotic synchronization are known such as complete and lag–synchronization [24,25], phase synchronization [3,26], generalized synchronization [27,28], time-scale synchronization [29,30] and others. Various methods of analysis should be used to detect different synchronization regimes in coupled systems and complex networks, and different measures of synchronization have been proposed for the quantitative characteristics of the synchronous regime onset [29,31–35].

[a] e-mail: hramovae@gmail.com

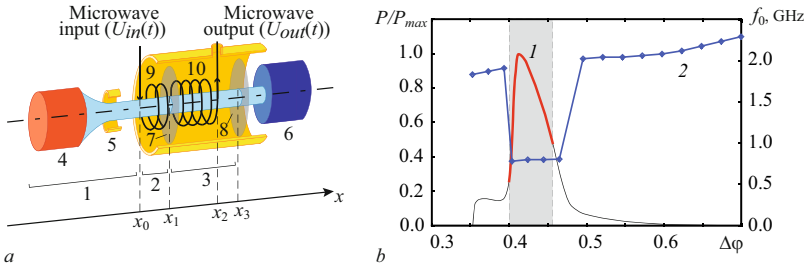

Fig. 1. (a) Schematic diagram of low-voltage vircator used as element of nonlinear antenna and (b) the normalized output power (curve 1, scale on LH axis) and basic frequency (curve 2, scale on RH axis) versus breaking potential $\Delta\varphi$ of autonomous vircator for $\alpha = 0.9$. Details of the vircator scheme: 1 – electron gun; 2 – modulation space; 3 – interaction space; 4 – cathode; 5 – anode; 6 – collector; 7 – input grid; 8 – output grid; 9 – modulating helix line section; 10 – output transmission line.

Typically, the majority of works devoted to the cooperative dynamics and different types of synchronization in complex networks deal with the node elements characterized by a small number of degrees of freedom [36–39], although the networks of the spatiotemporal systems became the object of interest in the past years (e.g., spatiotemporal networks have been studied in application to chemical reactions [40] and Pierce plasma diodes [41] recently). In this paper we extend the study of synchronization phenomena in the complex networks to the case of spatially extended coupled chaotic systems with the different topology of links between nodes. We propose the index of time scale synchronization in the network of complex oscillators for the quantitative characteristic of synchronous cluster formation. As such element of the network we consider the distributed model of new perspective device of microwave electronics called the low-voltage vircator demonstrating different nonlinear phenomena including chaotic microwave generation [42–46].

2 General formalism

Low-voltage vircator is a plane diode gap being penetrated by the electron beam with the overcritical perveance in the diode range [42]. To form the overcritical perveance the output grid of the system is subjected to the retardant potential the increase of which results in the virtual cathode (VC) (i.e., the potential barrier reflecting the part of electrons backwards to the injection plane) formation in the electron beam [47–51].

The considered model of vircator is shown schematically in Fig. 1(a). The system consists of electron source 1, section 2 of the pre-modulation of the electron beam, interaction space 3 with retarding potential where VC is formed in the electron beam, and collector 6.

The single velocity electron beam with current I_0 formed by the electron gun 1 with cathode 4 and anode 5 enters the area of the pre-modulating helix system 2. In this space, the electron beam is affected by the output signals of other vircators of the network. The external signal leads to the velocity modulation of electron beam passed through Sect. 2. The beam then emerges in the interaction space 3 of vircator. VC oscillations were registered with the help of the section of the broadband transmission line 10 loaded on the one hand onto absorptive insert and onto the power output on the other. The potential of the input grid electrode 7 is equal to the anode potential, V_0, and the potential of the output grid 8 $V_b = V_0 - \Delta V$ varies from value $V_b/V_0 = 1$

($\Delta V = 0$, without braking) to $V_b/V_0 = -1$ ($\Delta V = 2V_0$, the braking voltage exceeds the accelerated one). Under effect of the braking field, a non-stationary VC is formed in the electron beam of the low-voltage vircator; the form and power of its oscillations essentially depend on the value of the braking potential, V_0, and beam current, I.

To simulate the nonlinear non-stationary processes in the charged particle beam with VC we use the non-stationary one-dimensional model of beam dynamics based on the self-contained system of motion equations (for the dynamics of charged particles of the beam) and Poisson equation for the field of space charge [52].

In the equations describing the electron beam dynamics the following dimensionless values are used: potential φ, intensity E of field of the space charge, space charge density ρ, charged particles velocity v, space coordinate x, and time t

$$x = \frac{x'}{L}, \quad v = \frac{v'}{v_0}, \quad t = \left(\frac{v_0}{L}\right) t', \quad \rho = \frac{\rho'}{\rho_0}, \quad E = \left(\frac{L\eta}{v_0^2}\right) E', \quad \varphi = \left(\frac{\eta}{v_0^2}\right) \varphi'. \quad (1)$$

Here, stressed values correspond to the dimensional values, $\eta = e/m_e$ is the specific charge of electron, $v_0 = \sqrt{2\eta V_0}$ and ρ_0 are static (non-perturbed) velocity and density of electron beam at the input of the modulator, L is the drift space length. To estimate the dimension parameters of microwave generation we have considered the low-voltage vircator with the following values of basic control parameters: beam current $I_0 = 1.2\,\mathrm{A}$ and voltage $V_0 = 10\,\mathrm{kV}$, the length of interaction space $L = 25\,\mathrm{mm}$.

The numerical modelling of the non-stationary processes was realized with the help of the particle-in-cell (PIC) method [52]. The electron beam is considered as a set of large particles. In dimensionless variables the non-relativistic motion equation for each particle is given by:

$$\frac{d^2 x_i}{dt^2} = -E\left(x_i\right), \quad (2)$$

where x_i is the coordinate of i^{th} charged particle, $E(x_i)$ is the space-charge field intensity in the coordinate x_i.

The calculation of the electron beam density has been performed by PIC-method which consists in the following. To find the space charge the bilinear weighing [52] of the particle charge on grid has been performed. Then the space charge density in the cell j of the space grid, i.e., in $x_j = j\Delta x$ is given by

$$\rho(x_j) = \frac{1}{n_0} \sum_{i=1}^{G} \Theta(x_i - x_j), \qquad \Theta(x) = \begin{cases} 1 - |x|/\Delta x, & |x| < \Delta x, \\ 0, & |x| > \Delta x \end{cases} \quad (3)$$

where G is the full number of particles, n_0 is the numerical scheme parameter which is equal to the number of particles being in the unperturbed state in cell, Θ is the piecewise linear function defined by the procedure of "weighing" of particle in the space grid with the step Δx.

The intensity and potential of the space-charge field are defined on the uniform space grid with the step Δx. The space-charge field potential is determined by Poisson equation [52] which in 1D approximation takes a form

$$\frac{d^2 \varphi}{dx^2} = \alpha^2 \rho\left(x\right), \quad (4)$$

where $\alpha = \omega_p L/v_0$ is the Pierce parameter which is proportional to the square root of the beam current, $\alpha \sim \sqrt{I}$ [50] (ω_p is the plasma frequency). The boundary condition for Poisson equation is the requirement of the presence of the retardant potential difference between grids of the system, i.e. $\varphi(x_1) = 1$, $\varphi(x_3) = 1 - \Delta\varphi$ (see Fig. 1(a)).

The intensity of the space-charge field E is defined in such case by the numerical differentiation of the obtained values of the potential $E = -\partial\varphi/\partial x$.

The pre-modulating and output helix lines have been simulated using the interactive beam-circuit method [53]. According to this method, the transmission line has been described by the equations of telegraphy with the additional term defining the excitation of the electromagnetic waves by the beam

$$\frac{\partial I_{1,2}}{\partial t} = -\frac{1}{L}\frac{\partial U_{1,2}}{\partial x}, \qquad \frac{\partial U_{1,2}}{\partial t} = -\frac{1}{C}\frac{\partial I_{1,2}}{\partial x} + \frac{1}{C}\frac{\partial \rho}{\partial t}, \tag{5}$$

where $U_{1,2}(x,t)$ is the voltage and $I_{1,2}(x,t)$ is the current in pre-modulation (1) and output (2) transmission line sections, $\partial\rho/\partial t$ is beam charge variation. The equations of telegraphy have been solved numerically on the assumption of the feed line conditioning on the left $x = x_1$ and right $x = x_2$ edges of the transmission line.

In such model the output signal of vircator is $U_{out}(t) = U_2(x = x_2, t)$, and the input external signal affected vircator is described as $U_1(x = x_0, t) = U_{in}(t)$ where in our case $U_{in}(t)$ can be the sum of the output signals of other vircators of the network.

For example, Fig. 1(b) illustrates the output microwave power $P = \frac{1}{RT}\int_0^T U_{out}^2(t)dt$ (R is a loaded resistance) and the basic frequency of the output signal of the autonomous vircator with $\alpha = 0.9$ (that corresponds to the basic control parameter values mentioned above). One can see that the output power and frequency are essentially depended on the braking potential $\Delta\varphi$.

To analyze the time scale synchronization regime in the network of coupled low-voltage vircators we have made the numerical simulation of Eqs. (2)–(5) for each element of the network. The coupling between them has been realized by the assignment of the following boundary conditions for each element of the network

$$U_{\text{in}\,i}(x = 0, t) = \varepsilon \sum_{j=1}^{N} c_{ij} U_{\text{out}\,j}(t - \tau), \tag{6}$$

where i is the number of elements of the network, N is the number of elements in the feedback loop, ε is the coupling parameter defining the level of power getting in the communication line between generators, τ is the delay in the communication circuit between generators (it has been supposed to be equal to $\tau = 0.01$ for all communication lines), $U_{\text{out}\,j}(t)$ are the high-frequency oscillations from the output of j^{th} generator of the network.

Coefficients c_{ij} of the coupling matrix define the topology of the network of the coupled low-voltage vircators. If generator i influences generator j, the value of $c_{ij} = 1$. If generator i does not interact with the element j, $c_{ij} = 0$. It should be noted that the values of coefficients c_{ij} define only the fact of the presence of coupling between elements, whereas the strength of it is determined by the parameter ε. Furthermore, the elements of the network are not assumed to influence on each other, i.e. all elements on the main diagonal are equal to zero ($\forall i : c_{ii} = 0$).

3 Time scale synchronization

The time scale synchronization regime [29] means the presence of the synchronous dynamics in a certain range $[s_1; s_2]$ of time scales s introduced by means of continuous wavelet transform [54,55]

$$W(s, t_0) = \frac{1}{\sqrt{s}} \int_{-\infty}^{+\infty} x(t)\psi^*\left(\frac{t - t_0}{s}\right) dt, \tag{7}$$

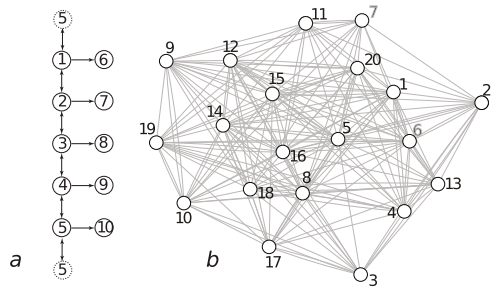

Fig. 2. Topologies of the networks under study. (a) The simply ordered chain, (b) the random network.

with Morlet complex mother wavelet function $\psi(\eta) = (1/\sqrt[4]{\pi})\exp(j\Omega_0\eta)\exp\left(-\eta^2/2\right)$, $\Omega_0 = 2\pi$. Using the complex wavelet basis we can characterize each of time scales by the phase $\phi(s,t) = \arg W(s,t)$, where $W(s,t)$ is the complex wavelet surface given by (7). The efficiency of the Morlet wavelet function for the introduction of phases of the time series of different nature (biological and electromagnetic signals) has been confirmed in the earlier studies [29,30,56–58]. For two coupled chaotic systems $\mathbf{x}_{1,2}(t)$ time scale synchronization takes place, if there is the range of the synchronous time scales $s \in [s_1; s_2]$ where the phase locking condition

$$|\phi_1(s,t) - \phi_2(s,t)| < 2\pi \tag{8}$$

is satisfied, and the part of the wavelet spectrum energy fallen on this range is not equal to zero $E_{snhr} = \int_{s_1}^{s_2} \langle |W(s,t)|^2 \rangle \, ds > 0$ [7,30,59].

4 Time scale synchronization in complex networks

Let us consider two different topologies of the networks of considered microwave oscillators. First of them corresponds to the simply ordered $N = 10$ chain of coupled generators whereas the second one is a random network of $N = 20$ elements, with low-voltage vircators being in their nodes. Figure 2 illustrates the topologies of the networks mentioned above. The first type of topology (i.e., the regular network) is typical for the active nonlinear antennas and phased arrays [10,11,15]. At the same time, the research focused on the study of networks of microwave oscillators with the random topology of links have not been conducted. We can expect the new effects in the collective dynamics of such random network in the microwave range. The number of their elements ($N = 10$ or $N = 20$) corresponds to the number of possible elements in real devices, e.g. used in the construction of the nonlinear active antennas [10] or the phased array of vircators [14,15,60]. Such number of elements allows effectively analyzing such networks of the spatially extended systems by means of the particle-in-cell method.

To analyze the time scale synchronization regime in the networks of the low-voltage vircators we have introduced the phases of output chaotic signals for each vircator on chosen time scale s (for the used Morlet wavelet the time scale s is connected with the frequency of oscillations as $f = 1/s$) and we have computed the phase differences for each pair (i,j) of the coupled generators in the network of N elements:

$$\forall i,j : 1 \le i,j \le N, i < j : \Delta\phi_{s\,ij}(t) = \phi_{s\,i}(t) - \phi_{s\,j}(t). \tag{9}$$

Two elements of the network are synchronized on time scale s if the phase difference $\Delta\phi_{s\,ij}(t)$ obeys Eq. (8), i.e. it is a time-limited function.

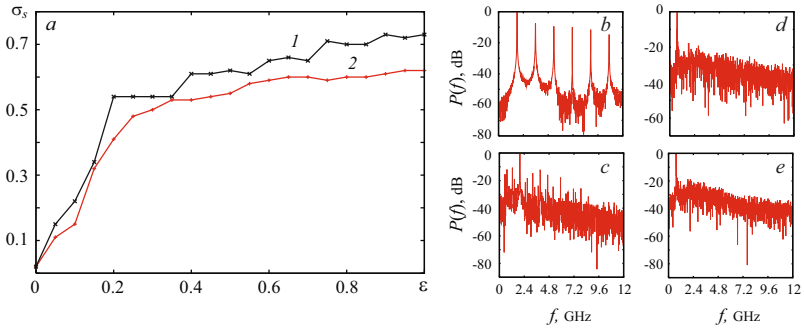

Fig. 3. (a) Dependencies of the synchronization index σ_s on the coupling parameter ε for the simply ordered chain of $N = 10$ low-voltage vircators with slightly (curve *1*) and strongly (curve *2*) detuned control parameter values. (b-e) Power spectra of output signals of first (b,d) and seventh (c,e) low-voltage vircators for the different values of the coupling parameter, i.e. $\varepsilon = 0$ (b,c), $\varepsilon = 0.2$ (d,e).

To characterize the degree of the synchronous state of the network quantitatively we have proposed to consider the time scale synchronization index, σ_s, on the chosen time scale for all network. Such index is similar to the last one proposed in [31] for two coupled systems and is given by

$$\sigma_s = \frac{1}{N_c} \sum_{i=1}^{N} \sum_{j=i+1}^{N} \sigma_{s_{ij}}, \tag{10}$$

where

$$\sigma_{s_{ij}} = \begin{cases} \dfrac{1}{T} \left| \displaystyle\int_0^T \exp\left[\sqrt{-1}\Delta\phi_{s\,ij}(t)\right] dt \right|, \; c_{ij} = 1 \vee c_{ji} = 1, \\ 0, \; c_{ij} = 0 \wedge c_{ji} = 0, \end{cases} \tag{11}$$

N_c is the number of pairs of coupled elements in the network (for which $c_{ij} = 1$ or $c_{ji} = 1$), T is the time of calculation. It is clear that σ_s can take the values being in the range from 0 to 1, with the limiting case $\sigma_s = 0$ being corresponded to the asynchronous time scale (i.e. all phase differences $\Delta\phi_{s\,i,j}(t)$ are distributed randomly on the $(0, 2\pi]$-interval [32]), whereas the extreme case $\sigma_s = 1$ being related to the case of synchronization of all elements of the network on the given time scale, s, when all phase differences obey relation (8). The intermediate values of synchronization index $0 < \sigma_s < 1$ correspond to the regimes of the formation of synchronous clusters in the network, when only part M of coupled elements of the network demonstrates the synchronous dynamics (i.e. the so-called synchronous cluster) whereas for all other $N - M$ coupled elements the synchronous state does not exist. Therefore, the growth of σ_s means that the network transits step-by-step to the synchronous dynamics through the increase of the number of elements in the synchronous cluster.

Let us describe the results obtained for the chosen topologies of the networks. We start our consideration with the simply ordered chain of low-voltage vircators (Fig. 2(a)). In Fig. 3(a) the dependencies of the synchronization index on the coupling parameter ε for such network and different values of the control parameters have been shown. Curve *1* corresponds to the case when the control parameter values for elements $1 - 5$ and $6 - 10$ are detuned slightly among themselves (i.e. $\alpha = 0.9$ for all elements, $\Delta\varphi = (0.37; 0.43; 0.40; 0.39; 0.42; 0.55; 0.53; 0.52; 0.51; 0.57)$) forming ipso facto two different clusters with closed values of the control parameters,

whereas curve *2* relates to the case of the strongly mismatched generators inside the second cluster ($\alpha = 0.9$, $\Delta\varphi = (0.37; 0.43; 0.40; 0.39; 0.42; 0.55; 0.6; 0.45; 0.36; 0.57)$).

For the selected values of the control parameters the autonomous low-voltage vircators demonstrate chaotic dynamics with the power spectra of oscillations of their space charge potentials being different according to the control parameter values (see, e.g. Figs. 3(b), (c) where the power spectra for the first and seventh elements of the slightly detuned chain in the absence of coupling have been shown). With the coupling parameter value increase the spectral structure of the signals changes remarkably and for $\varepsilon = 0.2$ their power spectra contain only one well-pronounced spectral component on the frequency $f = 0.78$ GHz (see, Figs. 3(d), (e)). Therefore, the synchronous regime has been analyzed only on the time scale $s = 1/f = 1.282$ ns corresponding to the main frequency of oscillations and the synchronization indices σ_s shown in Fig. 3 correspond just to that time scale.

Analysis of the dependencies of σ_s on the coupling parameter ε allows claiming that in the simply ordered chain of low-voltage vircators the step junction to the synchronous regime has been observed. It is connected with the fact that elements $1-5$ become synchronized considerably early than elements $6-10$ forming synchronous cluster in which all elements are synchronized with each other. At the same time, elements $6-10$ with unidirectional coupling enter in synchronism for the greater values of the coupling parameter strength ε. Indeed, it is clearly seen from Fig. 3(a) that in both considered cases the sharp increase of σ_s value up to $\sigma_s \approx 0.5$ has been observed. With the further increase of the coupling parameter microwave oscillators $6-10$ become synchronized step-by-step that is revealed by the appearance of the plateaux on the dependencies of the time scale synchronization index of the network on the coupling parameter which are clearly seen especially in curve *1*, Fig. 3(a). It is also clear that the time scale synchronization index is greater in the case of slightly mismatched parameters in the second cluster in comparison with the case of strongly detuned ones. Slightly mistuned generators are more easily synchronizable, which allows achieving synchronization of the whole network for the less values of the coupling strength between elements of the network.

Let us consider now a more interesting case of the network of $N = 20$ coupled low-voltage vircators, notably random network shown in Fig. 2(b). The control parameter values for the generators being in the nodes of the network have been selected in such a way that Pierce parameters α have been fixed for all elements of the network ($\alpha = 0.9$) whereas the retardant potentials $\Delta\varphi$ have been chosen arbitrary in the range $\Delta\varphi \in [0.4; 0.46]$ with the variance 0.0186 to be slightly mistuned. Selected range of the retardant potential values is marked by grey rectangle in the dependence of the output power of the autonomous low-voltage vircator on the value of $\Delta\varphi$ (see Fig. 1). It corresponds to the greatest values of the output power of the low-voltage vircator. At the same time, in this range vircators demonstrate the microwave oscillations with a lower frequency.

Figure 4(a) illustrates the dynamics of the time scale synchronization index for such network on the different time scales (the frequencies of the observation) with the increase of the coupling parameter value ε. It is clearly seen that in several cases the system demonstrates the gradual transition from the asynchronous dynamics to the time scale scale synchronization regime in the whole network.

The values of the frequencies of observation have been selected in the compliance with the spectral structure of the output signals. Figures 4(b)–(e) illustrates the evolution of the power spectra of the fifth low-voltage vircator of the network with the coupling parameter value increase. If the coupling strength is small enough ($\varepsilon = 0.15$) the power spectrum contains only one well-defined spectral component on the frequency $f = 0.752$ GHz (see Fig. 4(b)). The growth of the coupling parameter results in the essential complication of the spectral structure of the output signal,

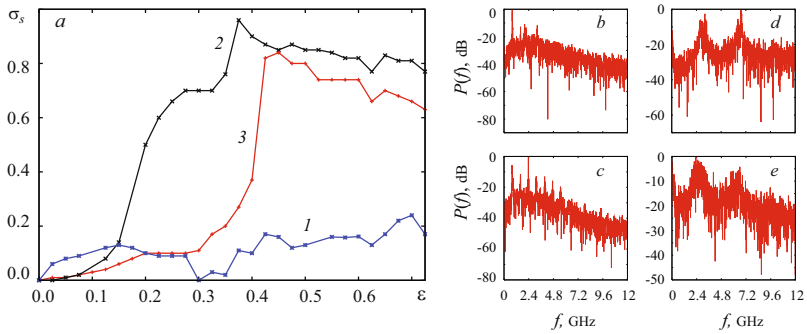

Fig. 4. (a) Dependences of synchronization index σ_s on the coupling parameter ε for the random network of $N = 20$ low-voltage vircators on the different frequencies (time scales) of observation, i.e. $f = 0.752\,\text{GHz}$ (curve *1*), $f = 2.67\,\text{GHz}$ (curve *2*), $f = 6.586\,\text{GHz}$ (curve 3). (b-e) Power spectra of output signals of fifth low-voltage vircator for the different values of the coupling parameter, i.e. $\varepsilon = 0.15$ (b), $\varepsilon = 0.275$ (c), $\varepsilon = 0.45$ (d), $\varepsilon = 0.775$ (e).

and for $\varepsilon = 0.275$ the additional spectral components are already appeared in it (see Fig. 4(c)). With the further increase of ε the most part of spectral components including the proper one ($f = 0.752\,\text{GHz}$) disappear and two well-defined spectral components (closed to $f = 2.67\,\text{GHz}$ and $f = 6.586\,\text{GHz}$) remain in the power spectrum (see Fig. 4(c) for $\varepsilon = 0.45$). These spectral components continue to exist with the further increase of ε (see Fig. 4(d) for $\varepsilon = 0.775$).

All three values of the frequencies mentioned above have been used for the calculation of the synchronization index (see Fig. 4(a)). Meanwhile, for the low-frequency component (curve *1*) the synchronization index begins firstly to increase, then it decreases down to zero and then continues to grow again. At the same time, the quantitative value of σ_s is small enough for all computed values of the coupling parameter strength. It means that only a small part of the coupled generators contains a synchronized spectral component on the frequency $f = 0.752\,\text{GHz}$ in contrast to the vircator chain considered above. For several values of the coupling parameter such spectral component is absent for all generators of the network and the synchronization index $\sigma_s = 0$. The increase/decrease of the value of the synchronization index indicates the appearance/disappearance of the corresponding synchronized spectral components in the power spectra of the output signals of the generators being in the nodes of the network.

On the contrary, the synchronization indices computed for two other spectral components (curve *2* and *3* in Fig. 4(a) demonstrate the behavior qualitatively identical to the last one obtained for the simply ordered chain of the coupled generators (see above). With the coupling parameter value increase the synchronization indices grow up to the values close to 1 indicating the time scale synchronization regime onset in the whole network of the coupled low-voltage vircators. The further growth of the coupling parameter strength results in the marginal changes of the quantitative values of the synchronization indices, i.e. both for $f = 2.67\,\text{GHz}$ and $f = 6.586\,\text{GHz}$ σ_s reaches the saturation level. At the same time, the small decrease of the value of σ_s connected with the small shift of the main frequencies of the oscillations takes place.

The gradual growth of the synchronization indices in the network under study allows assuming that the transition from the asynchronous state to the time scale synchronization regime in the whole network occurs via the formation of the synchronous cluster, with the number of its elements being increased with the growth of the coupling parameter. This fact is illustrated in Fig. 5 where the evolution of the synchronous cluster in the random network on the frequency $f = 2.67\,\text{GHz}$

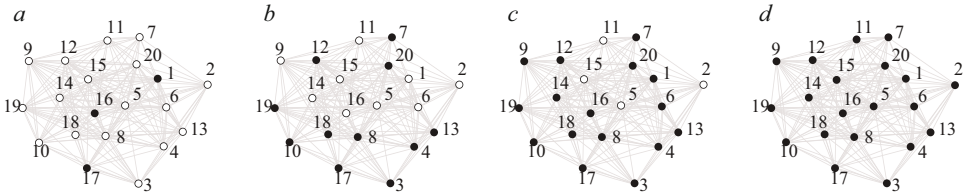

Fig. 5. The evolution of the synchronous cluster in the random network of $N = 20$ elements on the frequency $f = 2.67$ GHz with the coupling parameter value increasing: (a) $\varepsilon = 0.15$; (b) $\varepsilon = 0.225$; (c) $\varepsilon = 0.275$; (d) $\varepsilon = 0.375$. The asynchronous generators are shown by white circles, the generators being in the time scale synchronization regime are marked by black.

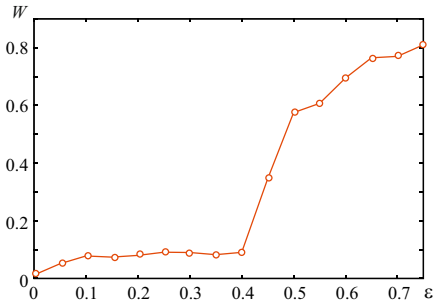

Fig. 6. Dependence of chaotic signal bandwidth W averaged over all oscillators of the network on the coupling parameter value ε.

(corresponding to curve *2*) has been shown. For the visualization of the synchronous cluster the asynchronous generators are shown by the white circles whereas the generators being in the time scale synchronization regime are marked by black. It is clearly seen that the number of the synchronous generators grows with the coupling parameter value increase, with the sharp jump of the number of the synchronous elements being realized at the small coupling parameter value variation (compare Figs. 5(a) and (b).

As we have mentioned above due to the influence of the several signals on the generators being in the nodes of the random network the spectral structure of the signals changes remarkably with their complication which took place. This is a new result, showing that in the random network of the weakly coupled chaotic microwave oscillators broadband chaotic signals can be generated in the synchronous regime, when there is the possibility of the effective summation of the microwave power of the different generators. Figure 6 illustrates the dependence averaged over all elements of the network of the chaotic signal bandwidth $W = \frac{1}{N}\sum_{i=1}^{N} \frac{\Delta f_i}{f_{0_i}}$ (where f_{0_i} is a proper frequency of the oscillations of i^{th} generator, Δf_i is the bandwidth of the chaotic signal of i^{th} generator) on the coupling parameter value. It is clearly seen that the characteristic increases sufficiently, and for the large values of the coupling parameter strength the oscillations in the generators become noise-like without the well-defined frequencies. In this case the network of the low-voltage vircators can be considered as a source of the powerful broadband GHz-radiation with the noise-like power spectrum. For example, such chaotic sources of microwaves can be used in the noise/chaotic radar technology [61,62] or atmospheric remote sensing [15,63]. Such technologies using the noise-like chaotic signals provide the excellent potential capabilities for Doppler measurements with the high resolution and accuracy. In addition, the chaos-based radar systems have the best low probability of the intercept

and electromagnetic compatibility performance, which enables designing of the cost-effective and affordable radar systems for the various applications, including atmospheric remote sensing, car radars, distance measuring systems, etc. [62–67].

5 Conclusions

In conclusion, we have analyzed the time scale synchronization regime in the networks of the coupled nonlinear elements with the different topologies of the links between nodes. As a node element of the network we have considered the one-dimensional distributed model of new perspective device of the microwave electronics, namely, the low-voltage vircator. To characterize the degree of synchronization in the whole network the time scale synchronization index has been introduced into consideration. We have shown that for both considered topologies of the networks (i.e., the simply ordered chain of the microwave oscillators and the random network) the transition from the asynchronous state to the time scale synchronization regime is accompanied by the formation of the synchronous cluster, with the number of its elements being increased with the growth of the coupling parameter strength. Moreover, the increase of the coupling parameter value results in the complication of the spectral structure of the signal that allows using such networks in the noise/chaotic radar technology.

This work has been supported by The Ministry of education and science of Russian Federation (14.B37.21.0751, 14.B37.21.1289, 14.B37.21.0059, government plan on 2013 and plan period of 2014 and 2015 years (SGTU-79)), Presidents programs (NSH-1430.2012.2, MD-345.2013.2, MK-672.2012.2), Russian foundation for basic researches (12–02–33071, 12–02–90022) and "Dynasty" Foundation.

References

1. V.S. Anishchenko, V.V. Astakhov, A.B. Neiman, T.E. Vadivasova, L. Schimansky-Geier, *Nonlinear Dynamics of Chaotic and Stochastic Systems. Tutorial and Modern Development*, 2nd edn. (Springer, 2007)
2. A.G. Balanov, N.B. Janson, D.E. Postnov, O.V. Sosnovtseva, *Synchronization: from simple to complex* (Springer, 2009)
3. A.S. Pikovsky, M.G. Rosenblum, J. Kurths, *Synchronization: a universal concept in nonlinear sciences* (Cambridge University Press, 2001)
4. F. Lau, C. Tse, *Chaos-Based Digital Communication Systems: Operating Principles, Analysis Methods, and Performance Evaluation* (Springer, 2003)
5. O.I. Moskalenko, A.A. Koronovskii, A.E. Hramov, Phys. Lett. A **374**, 2925 (2010)
6. A.A. Koronovskii, O.I. Moskalenko, A.E. Hramov, Physics-Uspekhi **52**, 1213 (2009)
7. A.E. Hramov, A.A. Koronovskii, P.V. Popov, I.S. Rempen, Chaos **15**, 013705 (2005)
8. B.S. Dmitriev, A.E. Hramov, A.A. Koronovskii, A.V. Starodubov, D.I. Trubetskov, Y.D. Zharkov, Phys. Rev. Lett. **102**, 074101 (2009)
9. H. Nijmeijer, Physica D-Nonlinear phenomena **154**, 219 (2001)
10. B.K. Meadows, T.H. Heath, J.D. Neff, et al., Proc. IEEE **90**, 882 (2002)
11. R.A. York, Z.B. Popovic, *Active and Quasi-Optical Arrays for Solid State Power Combining*, Microwave and Optical Engineering (New York: Wiley, 1997)
12. R. Ram, R. Sporer, *Chaos in microwave antenna arrays*, in *IEEE MTT-S Int. Microwave Symp. Dig.* (San Francisco, CA: IEEE, 1996), p. 324
13. K.C. Lee, T.H. Chu, Electromagnetic Compatibility, IEEE Trans. **47**, 963 (2005), ISSN 0018-9375
14. I.I. Magda, Y. Prokopenko, *Proc. 11th Int. Conf. High Power Particle Beams*, Prague, Czech Republic, Vol. 1 (1996), p. 422

15. A.E. Dubinov, V.D. Selemir, J. Commu. Tech. Electronics **47**, 575 (2002)
16. V.S. Anishchenko, T.E. Vadivasova, D.E. Postnov, M.A. Safonova, Int. J. Bif. Chaos **2**, 633 (1992)
17. J.J. Lynch, R.A. York, IEEE Microwave Guided Wave Lett. **5**, 213 (1995)
18. O.V. Sosnovtseva, A.I. Fomin, D.E. Postnov, V.S. Anishchenko, Phys. Rev. E **64**, 026204 (2001)
19. T.E. Vadivasova, G.I. Strelkova, V.S. Anishchenko, Phys. Rev. E **63**, 036225 (2001)
20. R.A. Filatov, A.E. Hramov, A.A. Koronovskii, Phys. Lett. A **358**, 301 (2006)
21. W.L. Ditto, S.N. Rauseo, M.L. Spano, Phys. Rev. Lett. **65**, 3211 (1990)
22. M. Ding, W. Yang, V. In, W.L. Ditto, Phys. Rev. E. **53**, 4334 (1996)
23. Y. Braiman, J.F. Lindner, W.L. Ditto, Nature **378**, 465 (1995)
24. L.M. Pecora, T.L. Carroll, Phys. Rev. Lett. **64**, 821 (1990)
25. L.M. Pecora, T.L. Carroll, G.A. Jonson, D.J. Mar, Chaos **7**, 520 (1997)
26. M.G. Rosenblum, A.S. Pikovsky, J. Kurths, Phys. Rev. Lett. **76**, 1804 (1996)
27. N.F. Rulkov, M.M. Sushchik, L.S. Tsimring, H.D. Abarbanel, Phys. Rev. E **51**, 980 (1995)
28. O.I. Moskalenko, A.A. Koronovskii, A.E. Hramov, S. Boccaletti, Phys. Rev. E **86**, 036216 (2012)
29. A.E. Hramov, A.A. Koronovskii, Chaos **14**, 603 (2004)
30. A.E. Hramov, A.A. Koronovskii, Physica D **206**, 252 (2005)
31. V.S. Anishchenko, D.E. Postnov, Sov. Tech. Phys. Lett. **15**, 28 (1990)
32. P.A. Tass, et al., Phys. Rev. Lett. **81**, 3291 (1998)
33. A. Shabunin, V. Demidov, V. Astakhov, V.S. Anishchenko, Phys. Rev. E **65**, 056215 (2002)
34. A. Shabunin, V. Astakhov, J. Kurths, Phys. Rev. E **72**, 016218 (2005)
35. A.E. Hramov, A.A. Koronovskii, M.K. Kurovskaya, O.I. Moskalenko, Phys. Rev. E **71**, 056204 (2005)
36. S.N. Dorogovtesev, J.F. Mendes, *Evolution of Networks* (Oxford University Press, 2003)
37. S. Boccaletti, V. Latora, V. Moreno, M. Chavez, D.U. Hwang, Phys. Reports **424**, 175 (2006)
38. I.V. Belykh, V.N. Belykh, K. Nevidin, M. Hasler, Chaos **13**, 165 (2003)
39. S. Boccaletti, *Complex Networks: Structure and Dynamics* (Elsevier, 2006)
40. O.U. Kheowan, E. Mihaliuk, B. Blasius, I. Sendiña Nadal, K. Showalter, Phys. Rev. Lett. **98**, 074101 (2007)
41. A.E. Filatova, A.E. Hramov, A.A. Koronovskii, S. Boccaletti, Chaos: An Interdisciplinary J. Nonlinear Sci. **18**, 023133 (2008)
42. Y. Kalinin, A.A. Koronovskii, A.E. Hramov, E.N. Egorov, R.A. Filatov, Plasma Phys. Reports **31**, 938 (2005)
43. E.N. Egorov, Y. Kalinin, A.A. Koronovskii, A.E. Hramov, Technical Phys. **52**, 1387 (2007)
44. S. Gursharn, C. Shashank, IEEE Trans. Plasma Sci. **36**, 694 (2008)
45. A.E. Hramov, A.A. Koronovskii, S.A. Kurkin, Phys. Lett. A **374**, 3057 (2010)
46. R.A. Filatov, A.E. Hramov, Y.P. Bliokh, A.A. Koronovskii, J. Felsteiner, Phys. Plasmas **16**, 033106 (2009)
47. R.A. Mahaffey, P.A. Sprangle, J. Golden, C.A. Kapetanakos, Phys. Rev. Lett. **39**, 843 (1977)
48. A.N. Didenko, Y. Krasik, S.P. Perelugin, G.P. Fomenko, Technical Phys. Lett. **5**, 321 (1979)
49. N.N. Gadetskii, I.I. Magda, S.I. Naisteter, Y. Prokopenko, V.I. Tchumakov, Plasma Phys. Report **19**, 273 (1993)
50. D.I. Trubetskov, A.E. Hramov, *Lectures on Microwave Electronics for Physicists*, Vols. 1,2 (Fizmatlit, Moscow, 2003)
51. J. Benford, J.A. Swegle, E. Schamiloglu, *High Power Microwaves* (CRC Press, Taylor and Francis, 2007)

52. C.K. Birdsall, A.B. Langdon, *Plasma physics, via computer simulation* (NY: McGraw-Hill, 1985)
53. I.J. Morey, C.K. Birdsall, IEEE Trans. Plasma Sci. **18**, 482 (1990)
54. B. Torresani, *Continuous Wavelet Transform* (Paris: Savoire, 1995)
55. A.A. Koronovskii, A.E. Hramov, *Continuous Wavelet Analysis and its Applications* (In Russian) (Moscow, Fizmatlit, 2003)
56. R.Q. Quiroga, A. Kraskov, T. Kreuz, P. Grassberger, Phys. Rev. E **65**, 041903 (2002)
57. A.A. Koronovskii, A.A. Ovchinnikov, A.E. Hramov, Phys. Wave Phenom. **18**, 262 (2010)
58. M.O. Zhuravlev, A.A. Koronovskii, O.I. Moskalenko, A.A. Ovchinnikov, A.E. Hramov, Phys. Rev. E **83**, 027201 (2011)
59. A.E. Hramov, A.A. Koronovskii, Y. Levin, JETP **127**, 886 (2005)
60. W. Woo, J. Benford, D. Fittinghoff, B. Harteneck, D. Price, R. Smith, H. Sze, J. Appl. Phys. **65**, 861 (1989)
61. R.M. Narayanan, M. Dawood, IEEE Trans. Antennas Propagation **48**, 868 (2000)
62. K.A. Lukin, Telecomm. Radio Eng. **55**, 2440 (2001)
63. G.E. Peckham, Reports Progr. Phys. **54**, 531 (1991)
64. C.P. Lai, R.M. Narayanan, IEEE Trans. Aero. Electron **46**, 1716 (2010)
65. B.M. Horton, Proc. IRE **47**, 821 (1999)
66. K. Kulpa, K. Lukin, W. Miceli, T. Thayaparan, Radar, Sonar Navigation, IET **2**, 229 (2008), ISSN 1751-8784
67. R.M. Narayanan, X. Xu, Proc. SPIE **5113**, 503 (2003)